

# High Photovoltaic Efficiency in Bulk-Stacked One-Dimensional GeSe<sub>2</sub> van der Waals Crystal

Seoung-Hun Kang,<sup>1,2,3,\*</sup> Youngjae Kim,<sup>4,5,\*</sup> Bo Gyu Jang,<sup>6,†</sup> and Sejoong Kim<sup>7,‡</sup>

<sup>1</sup>*Department of Physics, Kyung Hee University, Seoul, South Korea*

<sup>2</sup>*Department of Information Display,*

*Kyung Hee University, Seoul, South Korea*

<sup>3</sup>*Research Center for Technology Commercialization,*

*Korea Institute of Science and Technology Information (KISTI), Seoul, South Korea*

<sup>4</sup>*School of Physics, Korea Institute for Advanced Study (KIAS), Seoul 02455, Korea*

<sup>5</sup>*Department of Semiconductor Physics,*

*Kangwon National University, Chuncheon 24341, Republic of Korea*

<sup>6</sup>*Department of Materials Science and Engineering,*

*Kyung Hee University, Yongin, Gyeonggi 17104, South Korea*

<sup>7</sup>*Department of Electronic and Electrical Convergence Engineering,*

*Hongik University, Sejong 30016, South Korea*

## Abstract

Germanium diselenide (GeSe<sub>2</sub>) has recently attracted substantial interest as a rare example of one-dimensional (1D) van der Waals material. Here, we investigate the photovoltaic potential of bulk-stacked GeSe<sub>2</sub> chains using first-principles calculations within the  $GW_0$  approximation and the Bethe–Salpeter equation (BSE) to capture quasiparticle and excitonic effects. The bulk GeSe<sub>2</sub> exhibits indirect  $GW$  band gaps of 1.92 eV (type-I) and 1.08 eV (type-II). Optical calculations show markedly stronger visible-light absorption in type-II, yielding a spectroscopically limited maximum efficiency (SLME) of  $\sim 25.6\%$  at a  $0.5\ \mu\text{m}$  thickness. Phonon and room-temperature ab initio molecular dynamics analyses indicate that type-II is dynamically stable, whereas type-I shows imaginary phonon modes, suggesting a propensity for structural distortion. These results identify type-II GeSe<sub>2</sub> as a promising stable absorber for thin-film photovoltaics with enhanced flexibility compared to typical 2D vdW systems.

---

\* These two authors contributed equally

† Corresponding author. Email: bgjang@khu.ac.kr

‡ Corresponding author. Email: sejoong@hongik.ac.kr

## I. INTRODUCTION

In the past decade, van der Waals (vdW) low-dimensional materials have attracted widespread attention because their intrinsic electronic, optical, and topological properties differ markedly from those of conventional three-dimensional (3D) bulk compounds [1–8]. Unlike 3D solids, where strong covalent or ionic bonds dominate, vdW systems consist of discrete building blocks such as two-dimensional (2D) layers or one-dimensional (1D) chains held together by relatively weak inter-component forces known as vdW interactions [9–16]. This weak vdW binding makes it possible to exfoliate individual sheets or chains [8] and to stack different layers with atomic precision [17, 18]. These capabilities enable designer heterostructures whose optoelectronic behavior can be tuned on demand [3, 7].

Much of the early work focused on 2D vdW materials, especially graphene [19] and transition metal dichalcogenide monolayers [2]. Recent studies have begun to explore truly 1D vdW crystals that naturally form as isolated chains rather than being carved from a parent-layered bulk [20]. Classic examples such as carbon nanotubes predate graphene and already showcase exceptional mechanical, electrical, and thermal performance [21]. Quasi-1D nanoribbons derived from 2D sheets have also been investigated for nanoelectronics and quantum devices [22]. Intrinsically 1D vdW materials, such as selenium or tellurium chains, also exist, without being synthesized from layered precursors [23]. These materials present new opportunities for fundamental research and technological applications, offering distinct electronic, optical, and topological characteristics not accessible in 2D or 3D frameworks [24].

Germanium diselenide ( $\text{GeSe}_2$ ) exemplifies this class of true 1D vdW materials. Each Ge atom coordinates four Se atoms to form a tetrahedral  $\text{GeSe}_4$  unit. The adjacent tetrahedra share a two-Se edge to produce an extended chain-like lattice [25? ]. Recently, an alternative  $\text{GeSe}_2$  chain topology was synthesized inside carbon nanotube templates, demonstrating that  $\text{GeSe}_2$  can adopt multiple 1D conformations at the nanoscale [25? ]. Both the naturally occurring and template-assisted  $\text{GeSe}_2$  chains, which are called type-I and type-II, respectively, exhibit semiconducting behavior. Standard density functional theory (DFT) predicts that the type-I and type-II isolated  $\text{GeSe}_2$  chains possess mean-field bandgaps of about 1.90 and 0.80 eV, respectively [25? ].

However, in 1D systems, reduced screening amplifies many-body effects that are not captured by mean-field DFT. Quasiparticle gaps typically increase when computed using

the  $GW$  approximation [26], and strong excitonic binding can further reshape optical spectra [27]. Since the  $\text{GeSe}_2$  chain gap lies within the solar-spectrum window, these materials could be promising for next-generation photovoltaics [28]. A reliable assessment of their optoelectronic performance requires an accurate treatment of electron–electron interactions.

In this study, we provide a comprehensive computational investigation to demonstrate that the stacked bulk structure of  $\text{GeSe}_2$  chains holds significant potential for photovoltaic applications. Given the reduced dimensionality of the constituent 1D  $\text{GeSe}_2$  chains, an accurate consideration of electron–electron interactions is essential to obtain reliable electronic and optical properties. To address this issue, we perform *ab initio* many-body perturbation theory calculations within the  $GW_0$  approximation, which go beyond the limitations of conventional mean-field DFT calculations. This approach provides a more accurate description of quasiparticle excitations and electronic screening effects, both of which play a crucial role in determining the optoelectronic behavior of the material. By analyzing the optical spectra of the  $\text{GeSe}_2$  chains, we further assess their photovoltaic efficiency using the spectroscopically limited maximum efficiency (SLME) metric [29]. Our SLME calculations reveal that the  $\text{GeSe}_2$  chain structure can achieve a photovoltaic efficiency of up to 25.63% when stacked to a thickness of  $0.5\ \mu\text{m}$ . This efficiency is comparable to or even exceeds that of well-established vdW 1D photovoltaic materials,  $\text{Sb}_2\text{S}_3$  and  $\text{Sb}_2\text{Se}_3$ , [30, 31], highlighting the potential of  $\text{GeSe}_2$ -based nanostructures for future solar energy conversion.

## II. COMPUTATIONAL DETAILS

All first-principles calculations were performed using the Vienna *Ab initio* Simulation Package (VASP) [32, 33] with the projector-augmented wave method (PAW) [34]. The exchange–correlation potential was treated within the generalized gradient approximation (GGA) in the Perdew–Burke–Ernzerhof (PBE) form [35]. We used the DFT-D3 dispersion correction to describe the inter-chain van der Waals interactions [36], and also verified the key results using the revised vdW-DF2 functional with B86R exchange (rev-vdW-DF2, also referred to as vdW-DF2-B86R) [37, 38], where the revised Becke exchange functional (B86R) [39] is adopted for the exchange functional and a non-local correction is described by the second version of nonlocal vdW-DF (vdW-DF2) [40, 41]. A plane-wave energy cut-off of 500 eV was used for expanding the Kohn–Sham wavefunctions. The Brillouin zone

(BZ) integrations used the  $\Gamma$ -centered  $15 \times 15 \times 15$  Monkhorst-Pack  $k$ -grid for structural relaxations and total energy calculations. All atomic positions and lattice parameters were relaxed until the residual Hellmann–Feynman forces on each atom were below  $0.01 \text{ eV}/\text{\AA}$  and the total energy change between successive ionic steps was less than  $10^{-5} \text{ eV}$ .

Starting from the ground state converged DFT-GGA, the quasiparticle energies were obtained using the single-shot  $G_0W_0$  approximation with self-consistent update for  $G$ , which is denoted by  $GW_0$  [42, 43]. In the  $GW_0$  calculations, 180 bands (occupied and unoccupied) were included to ensure the convergence of the self-energy. The screened Coulomb interaction  $W$  was treated within the plasmon-pole approximation [42], and the dielectric matrix was constructed on an  $8 \times 8 \times 8$   $k$ -point grid with a plane-wave cutoff of 211 eV for the response-function expansion.

To incorporate excitonic effects in the optical spectra, we solved the Bethe–Salpeter equation (BSE) on top of the  $GW_0$  quasiparticle energies [44–48]. The BSE Hamiltonian included the top 12 valence bands and the lowest 8 conduction bands. The electron–hole kernel was constructed using the same  $8 \times 8 \times 8$   $k$ -point sampling, retaining local-field effects. From the BSE solution, we extracted the imaginary part of the macroscopic dielectric function  $\varepsilon_2(\omega)$  for photon energies up to 10.0 eV. The resulting  $GW_0$ +BSE absorption spectrum was compared to the independent-particle result at the  $GW_0$  level—denoted by  $GW$ +RPA—to assess the impact of electron–hole interactions on optical properties [48].

### III. RESULTS AND DISCUSSION

Figure 1 shows the atomic structures of two bulk polymorphs of  $\text{GeSe}_2$ , each formed by stacking one-dimensional chains via van der Waals forces. In type-I  $\text{GeSe}_2$  (Fig. 1(a)), each germanium atom is coordinated to four selenium atoms, forming a  $\text{GeSe}_4$  tetrahedron. Neighboring tetrahedra share a two-selenium edge, resulting in a continuous 1D tetrahedral chain. In contrast, the recently synthesized type-II  $\text{GeSe}_2$  chain is built from pairs of edge-sharing tetrahedra, as shown in Fig. 1(b). These pairs repeat along the chain direction by sharing only selenium corners, producing a different connectivity pattern.

When these 1D chains are assembled into a bulk phase via vdW interactions, both type-I and type-II structures adopt triclinic unit cells. The lattice constants  $a_i$  ( $i = 1, 2, 3$ ) and the interaxial angles  $\theta_{ij}$  between the vectors  $\mathbf{a}_i$  and  $\mathbf{a}_j$  are listed in Table I. In each case, the

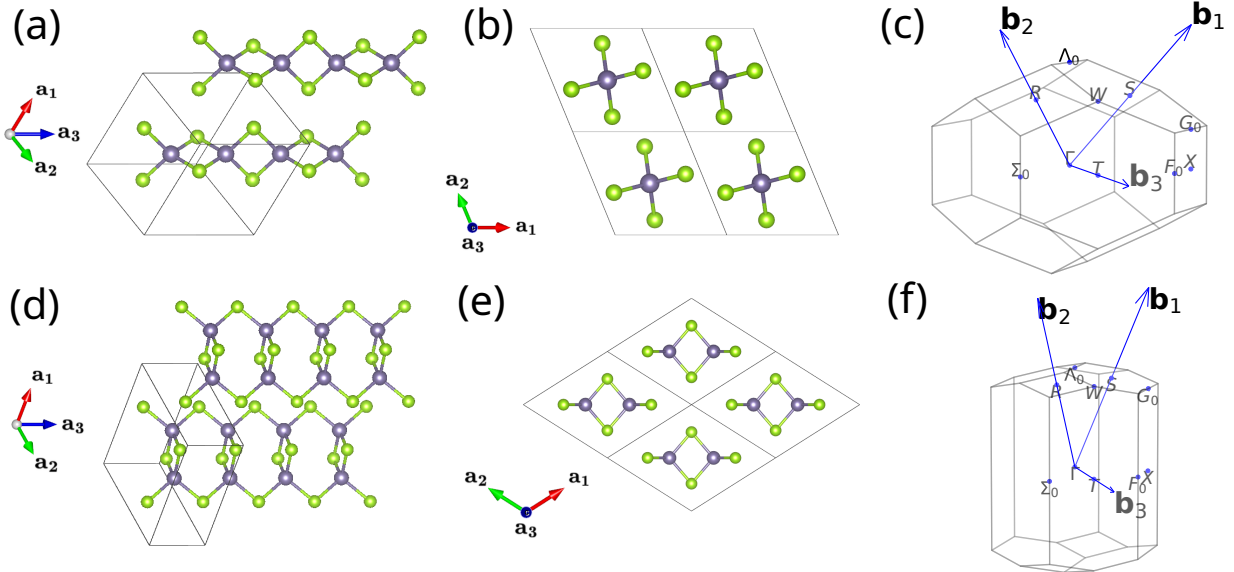


FIG. 1. (Color online) Atomic configurations of (a,b) type-I bulk  $\text{GeSe}_2$  and (d,e) type-II bulk  $\text{GeSe}_2$ . Triclinic primitive unit cells and corresponding lattice vectors  $\mathbf{a}_1$  (red),  $\mathbf{a}_2$  (green) and  $\mathbf{a}_3$  (blue) are illustrated with atomic chains. Corresponding irreducible Brillouin zones (IBZ) are illustrated for (c) type-I and (f) type-II chains. Reciprocal lattice vectors  $\{\mathbf{b}_1, \mathbf{b}_2, \mathbf{b}_3\}$  and high-symmetric points are displayed together. Atomic configurations are drawn by using VESTA [49].

chains run parallel to  $\mathbf{a}_3$ , and the in-plane lattice constants satisfy  $a_1 = a_2$ . Together, these parameters fully describe the triclinic geometry of the bulk  $\text{GeSe}_2$  phases derived from their respective 1D chains.

Accurate band-gap values are essential for assessing the photovoltaic potential of  $\text{GeSe}_2$ . To this end, we computed the band structures of both type-I and type-II bulk  $\text{GeSe}_2$  using

TABLE I. Lattice parameters for type-I and type-II bulk  $\text{GeSe}_2$ .

lattice parameters	type-I	type-II
$a_1$	6.3494 Å	7.2645 Å
$a_2$	6.3494 Å	7.2645 Å
$a_3$	6.3494 Å	7.2645 Å
$\theta_{12}$	$121.825^\circ$	$117.949^\circ$
$\theta_{23}$	$86.889^\circ$	$70.191^\circ$
$\theta_{31}$	$121.799^\circ$	$150.482^\circ$

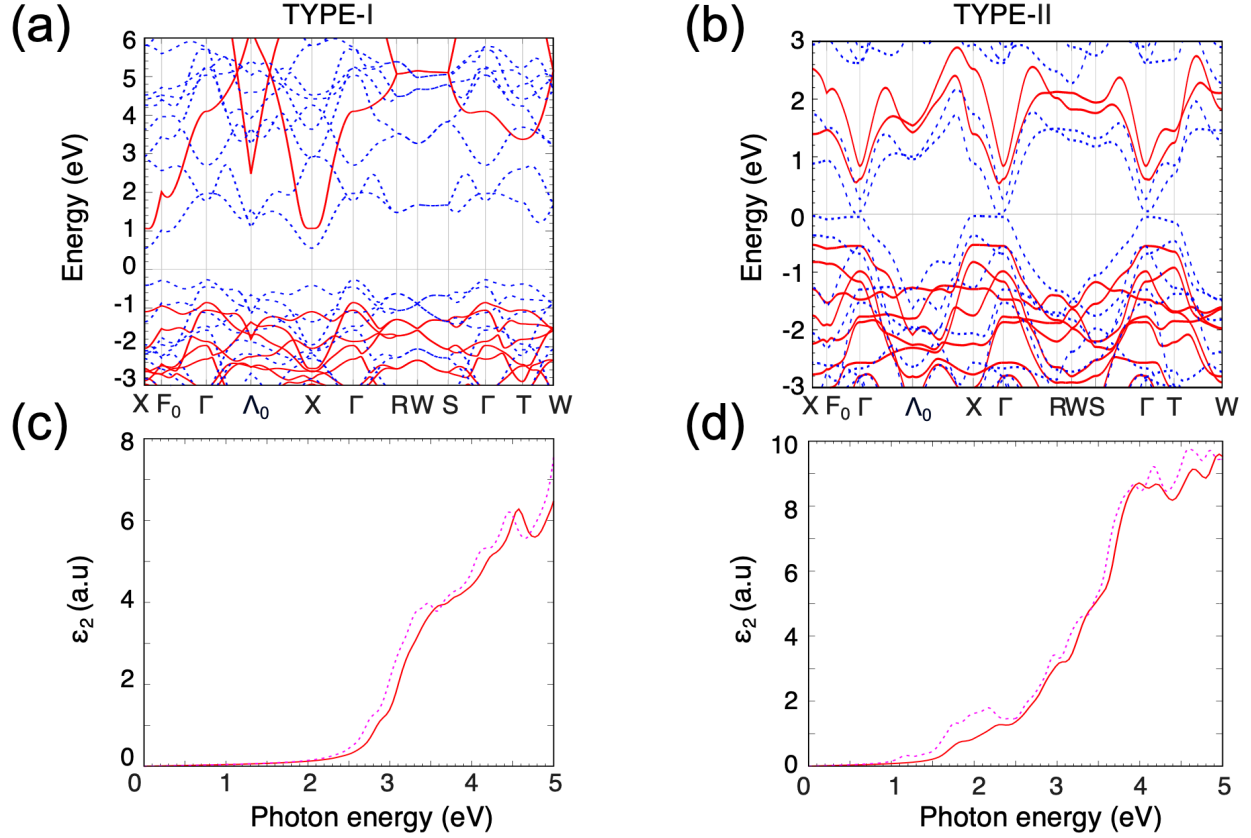


FIG. 2. Electronic structure of bulk type-I and type-II GeSe<sub>2</sub>. Electronic band structures computed by DFT-GGA (blue dashed) and *GW* (red solid) approximations for (a) type-I bulk GeSe<sub>2</sub> and (b) type-II bulk GeSe<sub>2</sub>. Absorption spectra  $\varepsilon_2$  from *GW* + BSE (magenta dashed) and *GW* + RPA (red solid) for (c) type-I bulk GeSe<sub>2</sub> and (d) type-II bulk GeSe<sub>2</sub>.

three approaches: DFT-GGA, the HSE06 hybrid functional [50, 51], and the  $GW_0$  approximation. Figures 2(a) and (b) represent the DFT-GGA and  $GW_0$  band structures for type-I and type-II GeSe<sub>2</sub>, respectively. Both polymorphs have an indirect fundamental gap located between the  $\Gamma$  and  $X$  points. The calculated band gaps are summarized in Table II.

When compared to the DFT-GGA band gaps of isolated 1D GeSe<sub>2</sub> chains, 1.91 eV for type-I and 0.79 eV for type-II [25], the bulk-stacked structures exhibit significantly smaller gaps at the GGA level as shown in Table II. In particular, type-II bulk GeSe<sub>2</sub> shows an extremely small GGA gap of 0.09 eV, indicating that 3D stacking enhances dielectric screening and consequently reduces the mean-field gap in comparison to low-dimensional cases.

Advanced calculations beyond the mean-field level yield band gaps larger than the GGA values. Compared to DFT-GGA calculations, HSE06 calculations enhance band gaps by

roughly 0.9 eV in both bulk polymorphs. The  $GW_0$  approximation predicts even larger band gaps. While for type-I  $\text{GeSe}_2$ , the  $GW_0$  approximation increases the band gap to 1.92 eV, it produces a gap for type-II  $\text{GeSe}_2$  (1.08 eV) slightly larger than the HSE06 value (1.00 eV). Figure 2 also shows that many-body corrections push the valence bands downward and the conduction bands upward compared to the mean-field result.

We use  $GW_0$  quasiparticle energies consistently for subsequent optical analyses. The optical absorption spectra were obtained by solving the Bethe–Salpeter equation (BSE) based on  $GW_0$  quasiparticle energies [44–48]. From the BSE solution, we extracted the imaginary part of the dielectric function,  $\varepsilon_2(\omega)$ , up to photon energies of 10.0 eV. Figures 2(c) and (d) compare the absorption spectra obtained with ( $GW+\text{BSE}$ ) and without ( $GW+\text{RPA}$ ) electron–hole interactions for type-I and type-II  $\text{GeSe}_2$ . The inclusion of electron–hole coupling through the BSE reveals excitonic features that are absent in  $GW+\text{RPA}$  spectra. For type-I, the  $GW+\text{BSE}$  calculation does not show low-energy excitonic peaks, whereas type-II exhibits a distinct excitonic peak around 2 eV. These results demonstrate that many-body effects are crucial for accurately modeling both the electronic band gaps and the optical response of bulk  $\text{GeSe}_2$  in the context of photovoltaic applications.

Figures 3(a) and (b) depict the calculated absorption coefficients  $\alpha(\omega)$  of type-I and type-II  $\text{GeSe}_2$  structures, respectively, overlayed with the standard AM 1.5 solar irradiance spectra [52]. Remarkably, type-II  $\text{GeSe}_2$  shows a substantially stronger absorption within the visible spectral range (highlighted by gray shading in Fig. 3) than its type-I counterpart. This enhanced absorption indicates a superior capability for photovoltaic energy conversion, attributed to optimal electronic transitions directly aligned with the energies of visible photons.

To quantitatively assess the photovoltaic potential, we computed the SLME metric [29],

TABLE II. Indirect (fundamental) band gap energies  $E_g$  for type-I and type-II bulk  $\text{GeSe}_2$  calculated by DFT+GGA, hybrid functional HSE06, and  $GW_0$  approximations.

calculation method	type-I	type-II
DFT+GGA	0.80 eV	0.09 eV
HSE06	1.69 eV	1.00 eV
$GW_0$	1.92 eV	1.08 eV

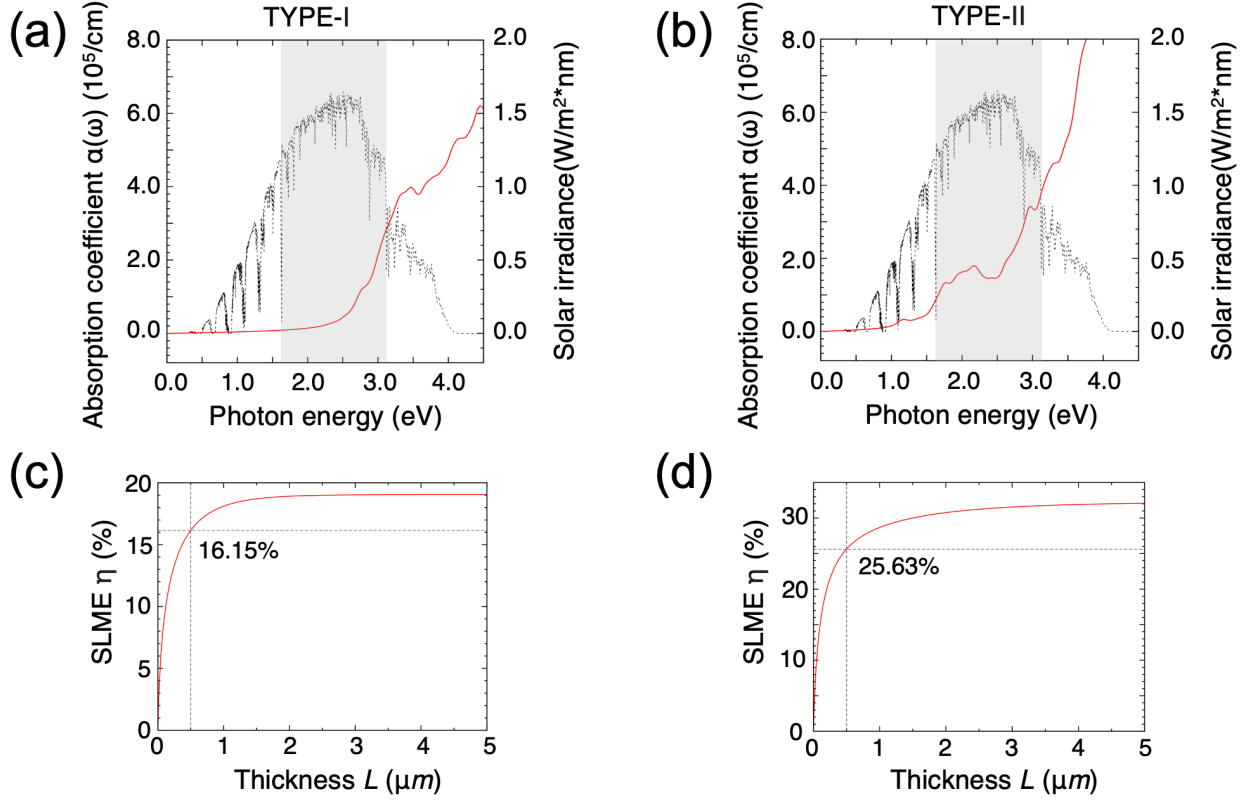


FIG. 3. Absorption coefficients (red solid line) of (a) type-I and (b) type-II bulk  $\text{GeSe}_2$ . The solar irradiance spectra, Air Mass 1.5, is shown with gray lines. The gray box specifies the energy range of visible light. The SLME  $\eta$  of (c) type-1 and (d) type-2 bulk  $\text{GeSe}_2$  are drawn as a function of thickness. For thickness  $0.5 \mu\text{m}$ , the values of SLME are explicitly indicated.

which provides realistic efficiency estimates by considering intrinsic optical absorption properties, electron-hole interactions, and recombination mechanisms. Figures 3(c) and (d) illustrate the SLME  $\eta$  as a function of absorber thickness  $L$  for both  $\text{GeSe}_2$  types. At a practical device thickness of  $0.5 \mu\text{m}$ , type-I  $\text{GeSe}_2$  demonstrates an SLME of approximately 16.15%, whereas type-II achieves an even higher efficiency of about 25.63%. The notably higher SLME for type-II  $\text{GeSe}_2$  underlines its exceptional promise as a photovoltaic absorber.

The predicted SLME of type-II  $\text{GeSe}_2$  (25.63% at  $0.5 \mu\text{m}$  thickness) places it in the upper range of efficiencies reported in recent SLME-based assessments of lead-free absorbers [29]. Similarly, computational screenings have suggested that some other lead-free candidates, such as layered  $\text{Si}_3\text{O}$  and delafossite-type  $\text{Cu}_2\text{ZnSnO}_4$ , may reach comparably high SLME values [53, 54].

Since  $\text{GeSe}_2$  is a bulk-stacked quasi-1D van der Waals material, a more direct comparison

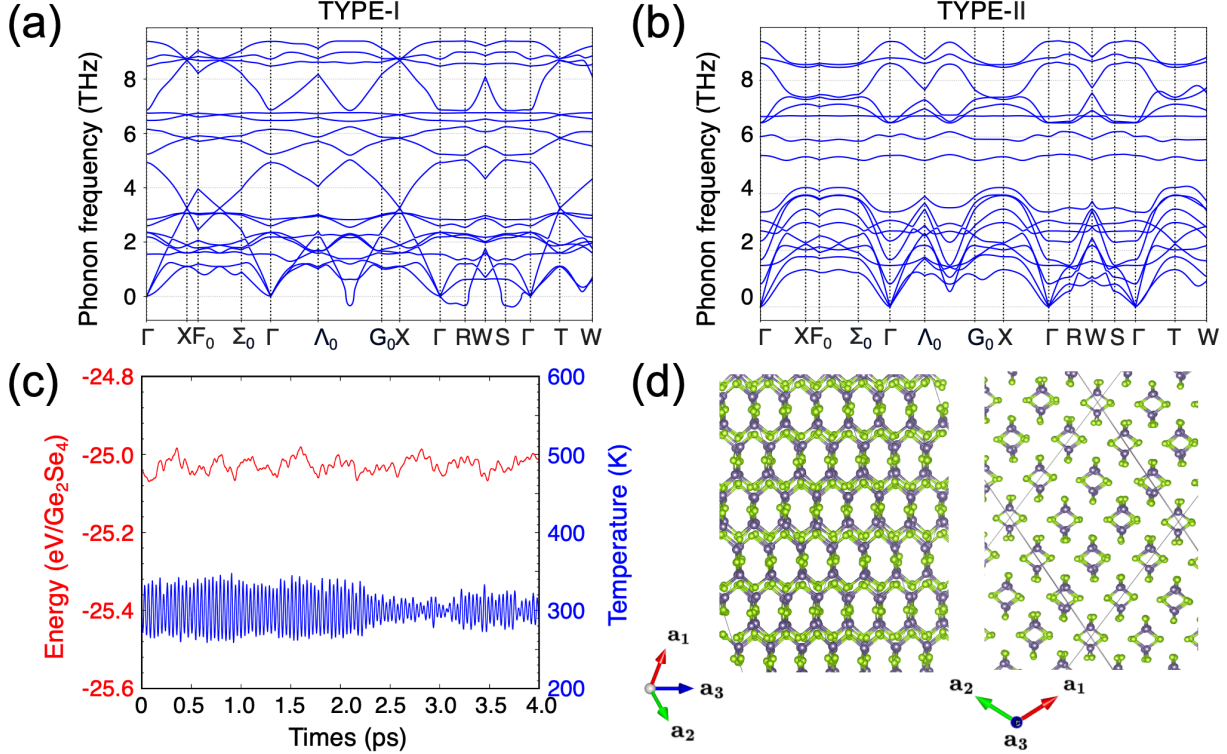


FIG. 4. Phonon frequencies of (a) type-I and (b) type-II bulk GeSe<sub>2</sub>. (c) Total potential energy and temperature as a function of time during canonical MD simulations at 300 K. (d) The final structure at the end of the simulation time of 4 ps (inset).

can be made with quasi-1D ribbon/chain chalcogenides such as Sb<sub>2</sub>Se<sub>3</sub> and Sb<sub>2</sub>S<sub>3</sub>, which have been widely investigated as thin-film photovoltaic absorbers [30, 31]. In particular, Sb<sub>2</sub>S<sub>3</sub> and Sb<sub>2</sub>Se<sub>3</sub> are reported to exhibit SLME values of approximately 23.5% and 29.0%, respectively, for a 0.5  $\mu$ m film thickness [55], indicating that type-II GeSe<sub>2</sub> is competitive within this broader class of quasi-1D van der Waals photovoltaic absorbers.

Having established the excellent photovoltaic efficiency and favorable optoelectronic characteristics of type-II GeSe<sub>2</sub>, it is crucial to verify its structural and thermal stability, as practical applications require materials to retain their properties under realistic operating conditions. To this end, we first assessed dynamic stability by calculating the phonon dispersion spectra for type-I and type-II GeSe<sub>2</sub>, as shown in Figs. 4(a) and (b). The phonon dispersion of type-I GeSe<sub>2</sub> exhibits imaginary (negative) frequencies in parts of the Brillouin zone, suggesting dynamical instability and a tendency toward structural distortions. By contrast, type-II GeSe<sub>2</sub> shows no imaginary frequencies across the Brillouin zone, supporting

its dynamical stability.

Although phonon calculations show harmonic structural stability at 0 K, they do not rule out the possibility of structural changes induced by thermal fluctuations at finite temperatures. Thus, to show robust thermal stability of type-II GeSe<sub>2</sub> structures at room temperature (300 K), we performed the *ab initio* molecular dynamics (AIMD) simulation [56]. Using the (3 × 3 × 3) supercell to include 27 formula units, AIMD was performed in the canonical ensemble (constant NVT). We controlled the temperature of the system by using the Nosé-Hoover thermostat [57, 58]. Figures 4(c) and (d) show the evolution of total potential energy and temperature over a 4-ps MD trajectory and includes snapshots of the final structures. Although small fluctuations in total potential energy are observed during the MD runs, no structural collapse or significant phase transformations occur, indicating that type-II GeSe<sub>2</sub> remains thermally stable over the simulated timescale at room temperature. Moreover, analysis of ensemble-averaged MD data confirms the achievement of thermal equilibrium within the simulation timeframe. Overall, these dynamic and thermodynamic stability analyses reinforce the viability of type-II GeSe<sub>2</sub> as a stable and efficient absorber material suitable for practical photovoltaic applications. These findings provide a robust theoretical basis to guide future experimental validation and optimization of GeSe<sub>2</sub>-based solar cells.

#### IV. CONCLUSION

In conclusion, our computational study identifies bulk-stacked type-II GeSe<sub>2</sub> as a promising photovoltaic absorber material, highlighting its superior optoelectronic properties and enhanced absorption. Utilizing *GW*+BSE calculations, we quantified the quasiparticle band gaps and excitonic effects, demonstrating that type-II GeSe<sub>2</sub> achieves an SLME of approximately 25.6% at 0.5  $\mu$ m absorber thickness. This efficiency is comparable to or superior to that of the leading emerging 1D photovoltaic materials stacked in bulk, such as Sb<sub>2</sub>Se<sub>3</sub> and Sb<sub>2</sub>S<sub>3</sub>. Crucially, phonon dispersion calculations and room-temperature molecular dynamics simulations confirm that type-II GeSe<sub>2</sub> phases are dynamically stable and thermodynamically robust, suitable for practical solar-cell applications. These findings underscore the promising potential of GeSe<sub>2</sub>-based nanostructures as next-generation photovoltaic materials and establish a theoretical foundation for subsequent experimental validation and device

integration.

## ACKNOWLEDGEMENT

S. Kim was supported by the National Research Foundation (NRF) of Korea (Grant no. NRF-2022R1F1A1074670, RS-2024-00410027 and RS-2025-16065427). B.G.J was supported by the National Research Council of Science & Technology(NST) grant by the Korea government (MSIT) (No. CAP25061-000) and the National Supercomputing Center with supercomputing resources, including technical support (KSC-2025-CRE-0367). Y.K. was supported by the National Research Foundation of Korea (NRF) grant funded by the Korea government (MSIT) (Grant no. RS-2025-00553820). Authors thank the computational support from the Center for Advanced Computation (CAC) at Korea Institute for Advanced Study (KIAS).

## CONFLICTS OF INTEREST

There are no conflicts to declare.

---

- [1] J. N. Coleman, M. Lotya, A. O'Neill, S. D. Bergin, P. J. King, U. Khan, K. Young, A. Gaucher, S. De, R. J. Smith, I. V. Shvets, S. K. Arora, G. Stanton, H.-Y. Kim, K. Lee, G. T. Kim, G. S. Duesberg, T. Hallam, J. J. Boland, J. J. Wang, J. F. Donegan, J. C. Grunlan, G. Moriarty, A. Shmeliov, R. J. Nicholls, J. M. Perkins, E. M. Grieveson, K. Theuwissen, D. W. McComb, P. D. Nellist, and V. Nicolosi, *Science* **331**, 568 (2011).
- [2] S. Z. Butler, S. M. Hollen, L. Cao, Y. Cui, J. A. Gupta, H. R. Gutiérrez, T. F. Heinz, S. S. Hong, J. Huang, A. F. Ismach, E. Johnston-Halperin, M. Kuno, V. V. Plashnitsa, R. D. Robinson, R. S. Ruoff, S. Salahuddin, J. Shan, L. Shi, M. G. Spencer, M. Terrones, W. Windl, and J. E. Goldberger, *ACS Nano* **7**, 2898 (2013).
- [3] Q. H. Wang, K. Kalantar-Zadeh, A. Kis, J. N. Coleman, and M. S. Strano, *Nature Nanotechnology* **7**, 669 (2012).
- [4] C. Tan, X. Cao, X.-J. Wu, Q. He, J. Yang, X. Zhang, J. Chen, W. Zhao, S. Han, G.-H. Nam, M. Sindoro, and H. Zhang, *Chemical Reviews* **117**, 6225 (2017).
- [5] A. Splendiani, L. Sun, Y. Zhang, T. Li, J. Kim, C.-Y. Chim, G. Galli, and F. Wang, *Nano Letters* **10**, 1271 (2010).

- [6] K. F. Mak, C. Lee, J. Hone, J. Shan, and T. F. Heinz, *Phys. Rev. Lett.* **105**, 136805 (2010).
- [7] A. K. Geim and I. V. Grigorieva, *Nature* **499**, 419 (2013).
- [8] K. S. Novoselov, A. K. Geim, S. V. Morozov, D. Jiang, Y. Zhang, S. V. Dubonos, I. V. Grigorieva, and A. A. Firsov, *Science* **306**, 666 (2004).
- [9] J. A. Wilson, F. J. Di Salvo, and S. Mahajan, *Adv. Phys.* **24**, 117 (1975).
- [10] K. S. Novoselov, A. K. Geim, S. V. Morozov, D. Jiang, Y. Zhang, S. V. Dubonos, I. V. Grigorieva, and A. A. Firsov, *Proc. Natl. Acad. Sci. USA* **102**, 10451 (2005).
- [11] M. Chhowalla, H. S. Shin, G. Eda, L.-J. Li, K. P. Loh, and H. G. Zhang, *Nat. Chem.* **5**, 263 (2013).
- [12] S. Manzeli, D. Ovchinnikov, D. Pasquier, O. V. Yazyev, and A. Kis, *Nat. Rev. Mater.* **2**, 17033 (2017).
- [13] R. H. Friend and A. D. Yoffe, *Adv. Phys.* **36**, 1 (1987).
- [14] J. A. Wilson and A. D. Yoffe, *Adv. Phys.* **18**, 193 (1969).
- [15] X. Wang, Y. Wen, D. Borges, and J. Xiao, *Adv. Funct. Mater.* **28**, 1802651 (2018).
- [16] T. Heine, *Acc. Chem. Res.* **48**, 65 (2015).
- [17] C. R. Dean, A. F. Young, I. Meric, C. Lee, L. Wang, S. Sorgenfrei, K. Watanabe, T. Taniguchi, P. Kim, K. L. Shepard, and J. Hone, *Nature Nanotechnology* **5**, 722 (2010).
- [18] A. Castellanos-Gomez, R. van Leeuwen, M. Buscema, H. S. J. van der Zant, G. A. Steele, and W. J. Venstra, *2D Materials* **1**, 011002 (2014).
- [19] A. K. Geim and K. S. Novoselov, *Nature Materials* **6**, 183 (2007).
- [20] R. Xiang, T. Inoue, Y. Zheng, A. Kumamoto, Y. Qian, Y. Sato, M. Liu, D. Gokhale, J. Guo, K. Hisama, S. Yotsumoto, T. Ogamoto, H. Arai, Y. Kobayashi, H. Zhang, B. Hou, A. Anisimov, Y. Miyata, S. Okada, S. Chiashi, Y. Li, J. Kong, E. I. Kauppinen, Y. Ikuhara, K. Suenaga, and S. Maruyama, *Science* **367**, 537 (2020).
- [21] S. Iijima, *Nature* **354**, 56 (1991).
- [22] Y. Son, M. L. Cohen, and S. G. Louie, *Nature* **444**, 347 (2006).
- [23] A. W. Sleight, *Journal of Solid State Chemistry* **5**, 160 (1972).
- [24] A. A. Balandin, F. Kargar, T. T. Salguero, and R. K. Lake, *Materials Today* **55**, 74 (2022).
- [25] Y. Lee, Y. W. Choi, K. Lee, C. Song, P. Ercius, M. L. Cohen, K. Kim, and A. Zettl, *ACS Nano* **17**, 8734 (2023).
- [26] L. Hedin, *Physical Review* **139**, A796 (1965).

[27] C. D. Spataru, S. Ismail-Beigi, L. X. Benedict, and S. G. Louie, *Physical Review Letters* **92**, 077402 (2004).

[28] L. Tsakalakos, J. Balch, J. Fronheiser, Y. Zhang, A. Mrdula, M. Kelzenberg, M. Lewinsheetz, L. Ade, and R. Buhrman, *Applied Physics Letters* **91**, 233117 (2007).

[29] L. Yu and A. Zunger, *Phys. Rev. Lett.* **108**, 068701 (2012).

[30] R. Kondrotas, C. Chen, and J. Tang, *Joule* **2**, 857 (2018).

[31] A. Mavlonov, T. Razykov, F. Raziq, J. Gan, J. Chantana, Y. Kawano, T. Nishimura, H. Wei, A. Zakutayev, T. Minemoto, X. Zu, S. Li, and L. Qiao, *Solar Energy* **201**, 227 (2020).

[32] G. Kresse and J. Furthmüller, *Physical Review B* **54**, 11169 (1996).

[33] G. Kresse and D. Joubert, *Physical Review B* **59**, 1758 (1999).

[34] P. E. Blöchl, *Physical Review B* **50**, 17953 (1994).

[35] J. P. Perdew, K. Burke, and M. Ernzerhof, *Physical Review Letters* **77**, 3865 (1996).

[36] S. Grimme, J. Antony, S. Ehrlich, and H. Krieg, *The Journal of Chemical Physics* **132**, 154104 (2010).

[37] I. Hamada, *Phys. Rev. B* **89**, 121103 (2014).

[38] H.-J. Kim, S.-H. Kang, I. Hamada, and Y.-W. Son, *Phys. Rev. B* **95**, 180101 (2017).

[39] A. D. Becke, *The Journal of Chemical Physics* **85**, 7184 (1986).

[40] M. Dion, H. Rydberg, E. Schröder, D. C. Langreth, and B. I. Lundqvist, *Phys. Rev. Lett.* **92**, 246401 (2004).

[41] K. Lee, E. D. Murray, L. Kong, B. I. Lundqvist, and D. C. Langreth, *Phys. Rev. B* **82**, 081101 (2010).

[42] M. S. Hybertsen and S. G. Louie, *Physical Review B* **34**, 5390 (1986).

[43] M. Shishkin and G. Kresse, *Physical Review B* **74**, 035101 (2006).

[44] M. Röhlfing and S. G. Louie, *Physical Review Letters* **81**, 2312 (1998).

[45] S. Albrecht, L. Reining, R. Del Sole, and G. Onida, *Physical Review Letters* **80**, 4510 (1998).

[46] M. Röhlfing and S. G. Louie, *Physical Review B* **62**, 4927 (2000).

[47] G. Onida, L. Reining, and A. Rubio, *Reviews of Modern Physics* **74**, 601 (2002).

[48] L. X. Benedict, E. L. Shirley, and A. H. MacDonald, *Physical Review Letters* **80**, 4514 (1999).

[49] K. Momma and F. Izumi, *Journal of Applied Crystallography* **44**, 1272 (2011).

[50] J. Heyd, G. E. Scuseria, and M. Ernzerhof, *J. Chem. Phys.* **118**, 8207 (2003).

- [51] A. V. Krukau, O. A. Vydrov, A. F. Izmaylov, and G. E. Scuseria, *J. Chem. Phys.* **125**, 224106 (2006).
- [52] Reference solar spectral irradiance: Air mass 1.5 retrieved 19 june 2025, <https://www.nrel.gov/grid/solar-resource/spectra-am1.5>.
- [53] S. Kim, K. Chae, and Y.-W. Son, *Nanoscale* **12**, 15638 (2020).
- [54] S.-H. Kang, M. Kang, S. W. Hwang, S. Yeom, M. Yoon, J. M. Ok, and S. Yoon, *Nanomaterials* **13**, 3111 (2023).
- [55] L. J. Phillips, C. N. Savory, O. S. Hutter, P. J. Yates, H. Shiel, S. Mariotti, L. Bowen, M. Birckett, K. Durose, D. O. Scanlon, and J. D. Major, *IEEE Journal of Photovoltaics* **9**, 544 (2019).
- [56] R. Car and M. Parrinello, *Phys. Rev. Lett.* **55**, 2471 (1985).
- [57] S. Nosé, *The Journal of Chemical Physics* **81**, 511 (1984).
- [58] W. G. Hoover, *Phys. Rev. A* **31**, 1695 (1985).